Journal of Power Sources 240 (2013) 705–712

Contents lists available at SciVerse ScienceDirect

Journal of Power Sources

journal homepage: www.elsevier.com/locate/jpowsour

Effect of post-heat-treated NiO_x overlayer on performance of nanocrystalline TiO_2 thin films for dye-sensitized solar cells

Yi-Cheng Lin [a], Yi-Ting Chen [a], Pin-Chuan Yao [b,*]

[a] Department of Mechatronics Engineering, National Changhua University of Education, Changhua 50007, Taiwan
[b] Department of Materials Science and Engineering, Da-Yeh University, Dacun, Changhua 51591, Taiwan

HIGHLIGHTS

- TiO_2 electrodes are coated with a NiO_x overlayer by reactive DC magnetron sputtering.
- The basic NiO_x-coated surface favours N719 dye attachment.
- A NiO_x overlayer suppressed the photoelectrons transfer from TiO_2 to the electrolyte.
- DSSC conversion efficiency was enhanced readily by coating with a NiO_x overlayer.
- For TiO_2/NiO_x(vacuum), oxygen impurities other than lattice oxygen were found.

ARTICLE INFO

Article history:
Received 3 January 2013
Received in revised form
17 April 2013
Accepted 8 May 2013
Available online 22 May 2013

Keywords:
Dye-sensitized solar cells
NiO_x
Direct current magnetron sputtering
Overlayer
Impedance analysis

ABSTRACT

In this study, nanostructured TiO_2 electrodes are coated with a NiO_x overlayer by reactive direct currrent magnetron sputtering for dye-sensitized solar cells (DSSC). The effects of a 10-min heat treatment at 450 °C in a rapid thermal annealing system under vacuum, TiO_2/NiO_x(vacuum), and under ambient atmosphere, TiO_2/NiO_x(air), has been intensively investigated.

For a TiO_2/NiO_x(air) electrode, the cell conversion efficiency (η) can be enhanced substantially due to the 10% increase in amount of N719 dye adsorbed on TiO_2 surface as compared with a bare TiO_2 electrode. The basic NiO_x-coated surface favours dye attachment through its carboxylic acid groups since the isoelectric point (IEP) of NiO (pH 10.3) is higher than that of anatase TiO_2 (pH 6.2). Electrochemical impedance spectroscopy analysis (EIS) shows that a NiO_x overlayer suppresses the transport of photoelectrons from TiO_2 to the electrolyte. It is proposed that IEP of NiO_x(air) is higher than that of NiO_x(vacuum). The more basic TiO_2/NiO_x(air) surface leads to an increment in dye adsorption which consequently facilitates the transport of electrons at the TiO_2/dye interface and results in better light harvesting. For TiO_2/NiO_x(air) electrode, the best η of 7.31% with J_{sc} and V_{oc} of 24.2 $mAcm^{-2}$ and 0.80 V, respectively are obtained.

1. Introduction

Solar energy conversion by photoelectrochemical cells has been thoroughly studied for decades. Dye-sensitized solar cells (DSSC), as the next-generation solar cells, differ from the traditional semiconductor devices in that they separate the function of light absorption from charge carrier transport [1], and have been widely investigated due to their low production cost and potentially high conversion efficiency ever since its invention almost two decades ago. A typical device comprises a nano-porous wide-band-gap semiconductor film on transparent conducting oxides substrate (TCO) as photoanode, which is placed in contact with a redox electrolyte containing an iodide/triiodide couple. Attached to the surface of the nanocrystalline film is a monolayer of dye and a platinized TCO as the counter electrode [2]. The overall solar-to-electric conversion efficiency of a DSSC cell comprising a nanostructured TiO_2 film coated with Ru-complex dye having the structure $RuL_2(NCS)_2$, where L stands for 2,2′-bipyridyl-4,4′-dicarboxylic acid (also known as N3 dye), has reached 10% [3]. Since then, DSSCs have been placed as one of the promising alternatives to bulk silicon-based solar cell which is currently dominant in the market [4]. At present, much research has been devoted to improving their performance and to elucidating the charge separation and transport mechanisms [2,5–11]. Unlike conventional p–n junction solar cells, DSSC is endowed with high surface

* Corresponding author. Tel.: +886 4 8511247.
E-mail addresses: pinchuanyao@gmail.com, pcyao@mail.dyu.edu.tw (P.-C. Yao).

0378-7753/$ – see front matter © 2013 Elsevier B.V. All rights reserved.
http://dx.doi.org/10.1016/j.jpowsour.2013.05.031

area interface between the semiconductor and the electrolyte solution where light is absorbed directly at this interface by a monolayer of adsorbed dye whereas initial charge separation occurs without the need for carrier (or exciton) transport [5]. The high conversion efficiency was attributed to ultrafast electron injection from the excited states of Ru-complex dye to TiO_2 and a much slower charge recombination from TiO_2 to the oxidized dye molecules and redox electrolytes [6]. The lack of a substantial potential barrier at the interface between the nanoporous film and electrolyte renders it a major energy loss mechanism in DSSCs. However, by retarding the recombination of injected electrons in semiconductor thin films with the oxidized sensitizer molecules and the electrolytes, the cell efficiency could be effectively improved [7]. Zaban et al. proposed a core–shell double structure to form a TiO_2/Nb_2O_5 bilayer electrode which can effectively suppress back-electron transfer at the interface of the nanoporous TiO_2 and dye molecules [8,9]. The conduction band potential of the thin-shell Nb_2O_5 layer (0 V vs. NHE at pH 0) is ca. 100 mV more negative than that of the TiO_2 core film, thus forming an inherent energy barrier at its surface and leading to great improvements of V_{OC} and J_{sc}. Following this strategy, various shell materials, such as Al_2O_3 [10,12,13], $BaCO_3$ [14], $CaCO_3$ [11,15], MgO [16], Nb_2O_5 [12], SiO_2 [10], $SrTiO_3$ [17], ZnO [18], ZrO_2 [10] and even metal (Al, Mg, Zn) hydroxides [19], have been employed. The roles of these shell materials (or blocking layer), through transient decay study, revealed that they may retard the charge recombination of the photo-induced electrons [10,12] or act as a barrier to energetically separate the injected photoelectrons from oxidized dye molecules and triiodide ions in electrolytes, thus increasing lifetime of carriers as compared with those comprising pristine TiO_2 electrodes [7,12,15,20].

Thin films of nickel oxide are an important component of sensor films [21], catalysts [22], electrochromic devices [23], p-type TCO materials [24,25] and the recording layer for next-generation high-density optical disc [26]. In the past decade, NiO films had drawn much attention in DSSC-related studies. Lindquist et al. [27] employed dye-sensitized nanostructured p-type NiO film as a photocathode for a novel DSSC device structure. Bandara et al. [28] fabricated an n–p junction electrode made of n-type SnO_2 and p-type NiO as alternative working electrode for traditional TiO_2-based DSSC. They also demonstrate a solid-state DSSC with p-type NiO acting as a hole collector as well as a barrier for charge recombination [29]. However, the light-to-electricity conversion efficiencies of these n-TiO_2/p-NiO heterojunction devices, at the current stage, were still quite low, regardless whether the electrodes are bi-layered [30] or multi-layered [31]. In contrast, Mori et al. [32] prepared dye-adsorbed NiO solar cells with six different metal-free organic dyes. They found that all electrodes showed cathodic current at wavelengths where the light absorption of dye took place. This phenomenon indicates that hole injection occurred from the adsorbed dyes to the valence band of NiO. Li et al. [33] coated the TiO_2 electrode with NiO film by reactive DC magnetron sputtering. By depositing a 21-nm-thick NiO overlayer, the light-to-electricity conversion efficiency increases from 3.21 to 4.16%. Electrochemical impedance analysis showed that electron recombination at the TiO_2/dye/electrolyte interface is reduced owing to the slightly increased surface resistance at the TiO_2/NiO interface. Accordingly, a thin NiO layer can act as a barrier layer for charge recombination between the reduced dye and the electrons in the TiO_2 conduction band [28,29]. Kim et al. [34] had revealed that oxygen vacancies on the TiO_2 film were substantially reduced after undergoing oxygen plasma treatment. During the sputtering process, the argon plasma can enhance reaction activity while the oxygen plasma can decrease oxygen vacancies and create a hydrophilic surface to facilitate dye absorption and, as a result, the photovoltaic performance of the as-treated DSSC is effectively improved [13].

In this study, a nanoporous TiO_2 electrode was fabricated by a commercial P25 paste. To improve the performance of DSSCs, the TiO_2 electrode with an optimal thickness was coated with a NiO_x overlayer by pulse DC magnetron sputtering. The effects of heat treatment on the as-deposited NiO_x films, including the morphology, microstructures, dye-adsorption, photovoltaic characteristics and electrochemical properties, were investigated.

2. Experimental

2.1. Preparation of electrodes

A slurry of nanocrystalline TiO_2 paste was prepared by grounding in a porcelain mortar 4 g of TiO_2 powder (Degussa P25, Aldrich) and 0.25 g polyethylene glycol (PEG, MW = 20,000, Showa) with a small amount of water (~10 mL) containing 2,4-pentanedione (1 mL, Merck) to prevent aggregation of particles. Finally, 0.1 mL of Triton X-100 (Acros) was added to facilitate the spreading of the colloid on the substrate. The paste was deposited onto fluorine-doped tin oxide (FTO, 8–10 Ω sq^{-1}., C.P. Solar, Taiwan) by spin coating, followed by drying in an environmental chamber kept at 25 °C with relative humidity of 60% for 8 h to prevent cracking. This process was repeated several times until the desired thickness of precursor films was reached. The as-deposited films were then sintered in air at 450 °C for 30 min and labelled as bare TiO_2 electrodes. The thickness of the nanocrystalline TiO_2 film was estimated by SEM.

2.2. Deposition of NiO_x overlayer

NiO_x overlayer was deposited on the bare TiO_2 electrode (TiO_2/NiO_x) by pulsed direct current magnetron sputtering, using a nickel target (Applied Materials, 99.99%) as the source material. The sputtering chamber was pumped down to 6.6×10^{-4} Pa using a cryogenic pump in which argon was used as the sputtering gas. The Ni target was pre-sputtered by argon plasma for 5 min before deposition. The working distance between the substrate and target was 8.5 cm. The deposition parameters were DC power 100 W, 95% duty cycle with a substrate temperature of 85 °C (without intentional heating), working pressure of 1.3 Pa in a gas mixture of Ar/O_2 = 70/30. The deposition rate was 6 nm min^{-1} and the thickness of NiO_x was ~18 nm as determined by a stylus profilometer (Kosaka laboratory Ltd., ET3000). The as-deposited TiO_2/NiO_x electrodes were further heat treated at 450 °C for 10 min in a rapid thermal annealing system (RTA) under vacuum (abbreviated as TiO_2/NiO_x(vacuum)) and ambient atmosphere (abbreviated as TiO_2/NiO_x(air)), respectively.

2.3. Cell assembly and measurements

The electrodes with an active area of 0.25 cm^2 were immersed in ethanol containing 0.3 mM ruthenium dye (N719, Solarnix) for 24 h. A platinum film, 160 nm in thickness, sputtered onto the FTO was employed as the counter-electrode. The electrolyte solution comprised 0.1 M LiI (Alfa Aesar), 0.05 M I_2 (Showa), 0.6 M 1,2-dimethyl-3-propylimidazolium iodide (DMPII, J.T. Baker), 0.5 M 4-tert-butyl pyridine (4-TBP, Aldrich) in acetonitrile (ACN, Shimakyu). Cells were assembled by applying a 50-μm spacer (Surlyn 1702, Dupont), melted by heating on a hot plate at 100 °C [24].

X-ray diffraction (XRD) patterns were obtained on a Shimadzu XRD-6000 diffractometer, equipped with a thin film sample holder in the 2θ range between 20° and 70° at grazing incidence ($\theta = 1°$) using CuKα radiation (λ = 1.5405 Å). Field emission scanning

electron microscopy (FESEM) was conducted using a JEOL JSM-7401F with an operating voltage of 4.0 kV. Photovoltaic characteristics were measured with a Keithley 2400 source meter under illumination from a solar simulator composed of a 500 W Xe lamp and an AM 1.5 filter (Oriel). The optical absorbance spectra were recorded with an UV/VIS/NIR spectrophotometer (Shimadzu UV-1800). The chemical states of the films were investigated by X-ray photoelectron spectroscopy (XPS, ULVAC-PHI 5000) with the Al Kα X-ray source (1486.6 eV) typically set at 3 kV, 24.9 W and an angle of 45° was used in this experiment. Each sample was ion-etched by Ar^+ sputtering (1 kV acceleration voltage with a beam current of 10 mA) for 20 s before XPS analysis. The position of the C_{1s} peak was taken as a reference with a typical binding energy of 284.6 eV. Electrochemical impendence spectra (EIS) were measured with a CH Instrument electrochemical analyzer (6081B, USA) in the frequency region from 10 MHz to 65 kHz under illumination of a 60 W halogen lamp by applying sinusoidal perturbations of ±10 mV superimposed on the open-circuit voltage (V_{oc}). The EIS were simulated using Z-View software (Solartron) [30].

3. Results and discussion

The post-heat-treatment on the bare TiO_2 electrode is important for fabricating efficient DSSCs. To improve the electronic contact between the TiO_2 particles and particles/TCO oxides interface, this treatment was found to improve significantly the short-circuit photocurrent as well as the open-circuit voltage of the solar cell [3]. Usually, the as-deposited TiO_2 film was sintered at 450–550 °C in air. However, the electrical conductivity of In-doped SnO_2 glass substrate (ITO) significantly decreases when it is sintered at high temperature, especially as the temperature exceeds 350 °C [35]. In contrast, DSSCs using F-doped SnO_2 substrate (FTO) show good tolerance towards thermal attack, i.e., the sheet resistances of FTO is lower with higher fill factors under identical fabrication conditions [36,37]. When a TiO_2 paste is employed to fabricate DSSC electrodes, the post-heat treatment on the as-deposited films is crucial in forming sufficient sintering with least organic residues. Thus it is desirable, at first, to explore the influence of the heat-treatment on the bare TiO_2 electrodes. Table 1 summarized the results where the photovoltaic characteristics of DSSCs were compared with different treatment temperatures for a bare TiO_2 electrode with a thickness of 4.21 μm (3 spin-coating layers). It shows that post-heat-treatment is beneficial in enhancing the photocurrent of the cells. The low photocurrent of the sample calcined at low temperature, as reported by Hoshikawa et al. [38], could be attributed to that a lot of grain boundaries prevent the injected electrons from flowing smoothly. Consequently, most of the injected electrons are lost at the grain boundaries where they cannot be collected to the outer circuits. The TiO_2 nanoparticles must be sintered at high temperature to improve electronic contact and eliminate organic substances in the colloidal paste. This leads to the promotion of electron transport at the grain boundary of TiO_2 particles and particles/SnO_2 interface. In addition, the heat treatment will transfer a portion of the rutile crystalline into the anatase crystalline, resulting in better material properties for DSSCs application [39]. A maximum conversion efficiency of 2.79% is achieved with a post-heat-treatment temperature of 450 °C for 30 min in air. The photovoltaic performance deteriorates at 500 °C. As depicted in Fig. 1, the I–V curve of the cell at 500 °C, differs a lot as compared to the other three cells. The large decline in FF could be a sign of abrupt surge in series resistance (R_s) of the cell, as derived from analysis of equivalent circuit (EQC) for dye-sensitized solar cell, which correspond to the sum of three resistance elements [40]:

$$R_s = R_h + R_1 + R_3 \quad (1)$$

where R_h is the sheet resistance of FTO, R_1 related to the charge-transfer processes occurring at the Pt counter electrodes and R_3 related to carrier transport by ions within the electrolyte, respectively. Based on equation (1), the resistance element of R_h dominates the variation of FF which is similar to that derived for a conventional silicon solar cell [41].

The thickness of TiO_2 electrode is one of the crucial parameters affecting the performance of DSSCs. In general, a thicker TiO_2 film adsorbs a larger amount of dye. Shin et al. [42] reported that increase in TiO_2 thickness is accompanied by decrease in charge transfer resistance at the TiO_2/dye/electrolyte interface, thus extending the electron lifetime. This facilitates the diffusion and transport process for the injected electrons in the TiO_2 layer and results in improvement of cell efficiency. In contrast, a thick TiO_2 film might increase the charge recombination between injected electrons and electroactive agents arising from low drift mobility of electrons in the film (10^{-4}–10^{-7} cm V^{-1} s^{-1}), which limits the conversion efficiency [43]. In order to fabricate a TiO_2 electrode with sufficiently high conversion efficiency, multi-layered films deposited by spin-coating were optimized in a preliminary study. The J–V curves of the resultant TiO_2 electrodes tested under AM 1.5 illumination are shown in Fig. 2, and the detailed photovoltaic characteristics values are listed in Table 2. As can be seen, the short-circuit photocurrent density (J_{sc}) increased steadily up to the TiO_2 electrode with nine spin-coated layers. In light of open circuit voltage (V_{oc}) and filled factor (FF), these two values seem to be less sensitive to the thickness of TiO_2 film. Previous studies indicated that for DSSCs, the photovoltaic characteristics of J_{sc} were closely related to the thickness of TiO_2 films [43], but less related to that of

Table 1
Effect of post-heat-treatment temperature on the photovoltaic characteristics of DSSC (thickness of TiO_2 = 4.21 μm).

Temperature (°C)	V_{OC} (V)	J_{SC} (mA cm^{-2})	FF	η (%)
300	0.66	0.20	28.93	0.03
350	0.72	6.12	61.21	1.96
400	0.70	6.23	62.76	2.03
450	0.77	8.39	63.36	2.79
500	0.74	8.44	56.89	2.42

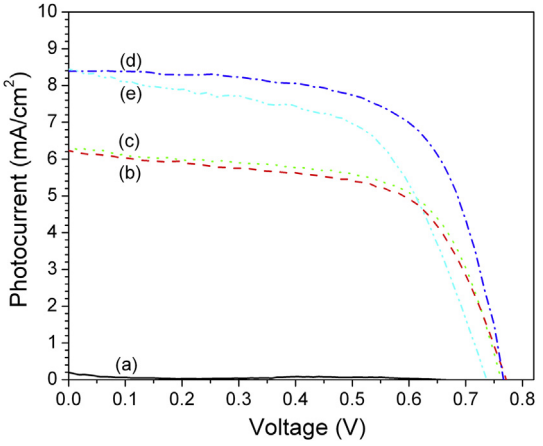

Fig. 1. I–V characteristics curves of DSSC with bare TiO_2 electrodes by varying the post-heat-treatment temperature under a solar simulator (AM 1.5, 100 mW cm^{-2}): (a) 300 °C, (b) 350 °C, (c) 400 °C, (d) 450 °C and (e) 500 °C.

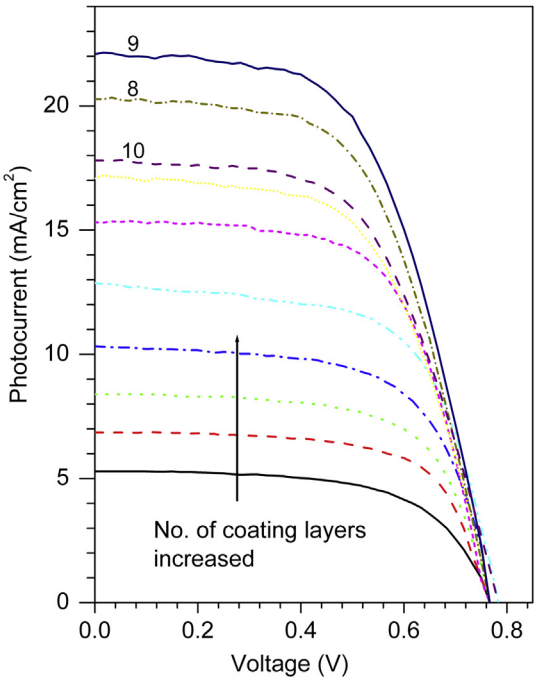

Fig. 2. *I–V* characteristics curves of DSSC with different TiO_2 electrodes by varying the number of spin-coated layers under a solar simulator (AM 1.5, 100 mW cm^{-2}).

V_{oc} [42,44]. For regenerative photoelectrochemical systems, the following relation holds [45]:

$$V_{oc} = \left(\frac{kT}{e}\right)\ln\left(\frac{\phi\Gamma_o}{n_{so}k_{et}\left[I_3^-\right]}\right) \quad (2)$$

where Γ_o is the incident photon flux, ϕ is the quantum yield for photogenerated electrons to reach the interface region, n_{so} is the equilibrium electron concentration at the TiO_2 surface, and k_{et} is the rate constant for the triiodide reduction.

Equation (2) indicates that V_{oc} is strongly dependent on $\phi\Gamma_o$, n_{so} and k_{et}, respectively. In general, k_{et} could be reduced by blocking the surface of TiO_2 with tert-butylpyridine (TBP) [3] or by an insulating oxide overlayer to suppress the dark current at the TiO_2-electrolyte junction [6]. In our study, as $\phi\Gamma_o$ was kept constant, the product of n_{so} and k_{et} dominates the resultant V_{oc}. EIS results, as proposed by Shin et al. [42], confirmed that k_{et} was reduced to a certain extent as the thickness of TiO_2 film was increased. Accordingly, it is reasonable that V_{oc} is larger, even in a minor amount, for thicker TiO_2 films. The amount of dye loadings of the P25 TiO_2 (not shown here) revealed that more N719 dye molecules were attached to the surface of TiO_2 for thicker films. The increase in J_{sc} is attributed to the fact that more photoelectrons were injected under light illumination by larger amount of attached dye [42], which results in a substantial improvement of incident-photon-to-current conversion efficiency (IPCE) for thicker TiO_2 films [43]. In our study, a TiO_2 electrode with an optimal thickness of 14.4 μm (9 layers) was employed for the following studies.

Table 2
Photovoltaic characteristics of DSSC with different TiO_2 thickness.

No. of spin-coated layers	Thickness (μm)	V_{OC} (V)	J_{SC} (mA cm^{-2})	FF	η (%)
1	1.26	0.77	5.13	0.63	1.63
2	2.70	0.77	6.87	0.63	2.25
3	4.21	0.77	8.23	0.63	2.79
4	5.69	0.77	10.32	0.63	3.33
5	7.24	0.77	12.86	0.65	4.59
6	8.55	0.76	15.52	0.63	4.96
7	10.57	0.78	17.68	0.64	5.16
8	12.71	0.78	20.41	0.64	5.93
9	14.41	0.78	22.08	0.65	6.89
10	16.38	0.79	17.92	0.63	5.34

The TiO_2/NiO_x electrodes, as characterized by the X-ray diffraction in Fig. 3, revealed that TiO_2 (anatase) dominated in all samples. No reflections that are attributable to the rutile phase could be identified. It is noteworthy that no diffraction peaks of NiO phase could be detected for TiO_2/NiO_x(vacuum). In contrast, minor NiO reflections are present even though the grazing incidence mode was carried out for TiO_2/NiO_x(air) [33].

The SEM micrographs in Fig. 4 revealed that all films were nanoporous in which the surface on the bare TiO_2 and TiO_2/NiO_x(vacuum) contained lots of voids and cavities. By annealing under ambient atmosphere, these voids diminished, as shown in Fig. 4(c), thus yielding a porous morphology with uniform and contiguous pores.

The photocurrent–voltage curve of cells in Fig. 5 shows the typical behaviour of the standard DSSC. A prominent effect on the current–voltage characteristics was exhibited after applying a NiO_x overlayer. For TiO_2/NiO_x(vacuum), the *J–V* curve lies underneath that of a bare TiO_2 electrode at identical bias voltage. In contrast, a NiO_x(air) underlayer improves substantially the photocurrent density under identical conditions. Detailed results of photovoltaic performance of the cells are summarized in Table 3. As can be seen, cell conversion efficiency (η) enhanced substantially for TiO_2/NiO_x(air) electrode. Moreover, a NiO_x overlayer also imparted an adverse effect on cell characteristics, i.e., the fill factor (FF) declined substantially for both electrodes with a NiO_x overlayer. However, the decline in FF was compensated and overwhelmed by J_{sc} and a highest efficiency of 7.31% was achieved for cells with a $TiO_2/$

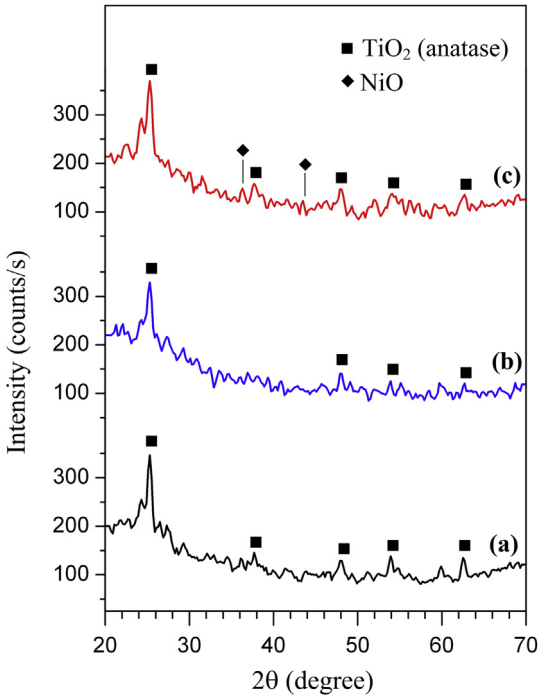

Fig. 3. X-ray diffractograms of (a) bare TiO_2, (b) TiO_2/NiO_x(vacuum) and (c) TiO_2/NiO_x(air).

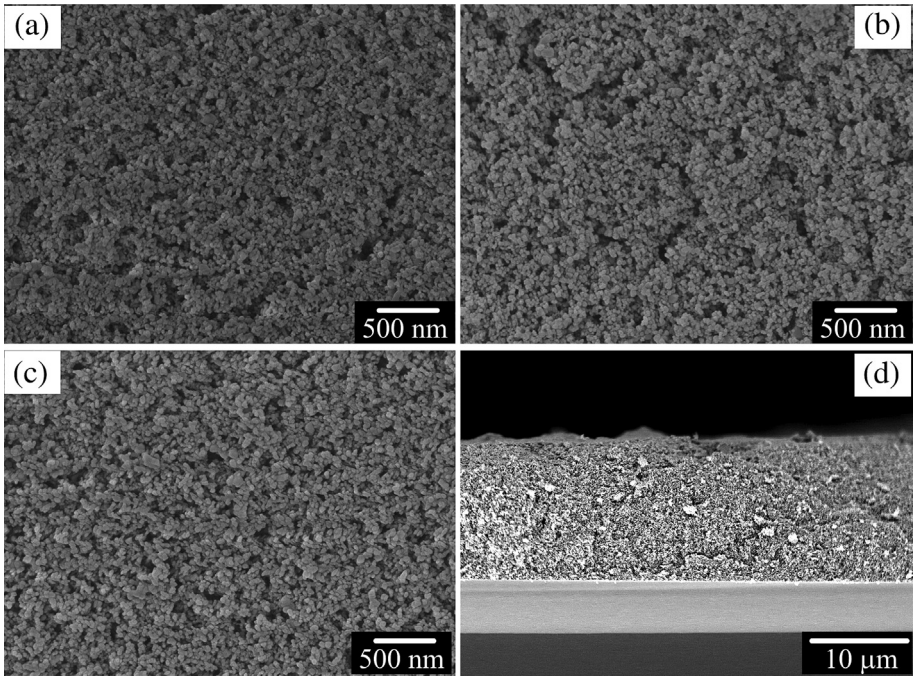

Fig. 4. SEM image of (a) bare TiO_2, (b) TiO_2/NiO_x(vacuum), (c) TiO_2/NiO_x(air) and (d) cross-sectional image of TiO_2/NiO_x(air).

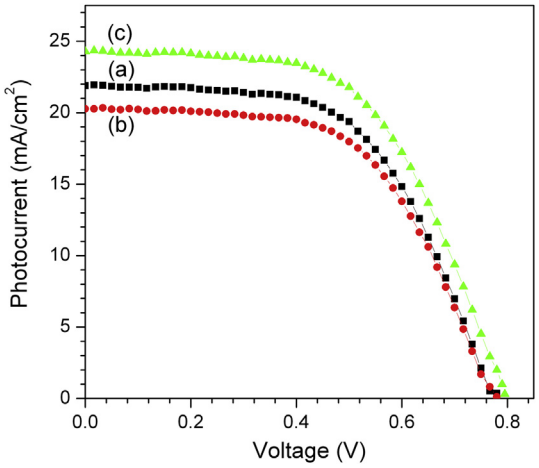

Fig. 5. Photovoltaic performance of three electrodes under a solar simulator (AM 1.5, 100 mW cm^{-2}): (a) bare TiO_2, (b) TiO_2/NiO_x(vacuum) and (c) TiO_2/NiO_x(air).

NiO_x(air) electrode, which shows a V_{oc} of 0.8 V, J_{sc} of 24.15 mA cm^{-2} and FF of 0.63, respectively.

To confirm further the effects of the NiO_x overlayer, the amount of N719 dye attached on the TiO_2 surface measured by UV–vis spectrophotometric determination of the dye solution was obtained by desorbing the N719 dye on the TiO_2 film into a 0.1 M NaOH solution. As seen in Fig. 6, an increase in dye adsorption was found upon the two TiO_2/NiO_x electrodes. The surface concentrations of N719 dye was determined as 5.608×10^{-8} mol cm^{-2} for the TiO_2/NiO_x(air) electrode, corresponding to a 10% increase in the amount of adsorbed dye for the bare TiO_2 (5.073×10^{-8} mol cm^{-2}) electrode. To elucidate the plausible explanation on the improvement of J_{sc}, a schematic picture of the TiO_2 surface with and without NiO_x overlayer was depicted in Fig. 7. As can be seen, by applying a NiO_x overlayer, the total amount of dye attached onto the TiO_2 surface increased owing to the extension of effective surface area of the whole electrode. A closer look at the performance of these two TiO_2/NiO_x electrodes revealed that the surface concentrations of N719 dye on the two electrodes were similar, but their photovoltaic characteristics differed a lot from each other. For N719 dye, the two carboxylic acid groups with bidentate coordination mode anchor onto the TiO_2 surface. The binding mode of N719 to the TiO_2 surface may influence dye adsorption and thus photovoltaic performance [46]. Previous studies indicated that an overlayer with highest isoelectric point (IEP) would be endowed with most basic film surfaces, which resulted in the highest dye adsorption [15]. Since the IEP of

Table 3
Photovoltaic performance of DSSCs fabricated with and without NiO_x overlayer.

	Cell area (cm^2)	V_{OC} (V)	J_{sc} (mA cm^{-2})	FF (%)	η (%)
Bare TiO_2	0.251	0.78	22.48	64.73	6.89
TiO_2/NiO_x(vacuum)	0.252	0.78	20.25	63.77	6.01
TiO_2/NiO_x(air)	0.249	0.80	24.15	62.71	7.31

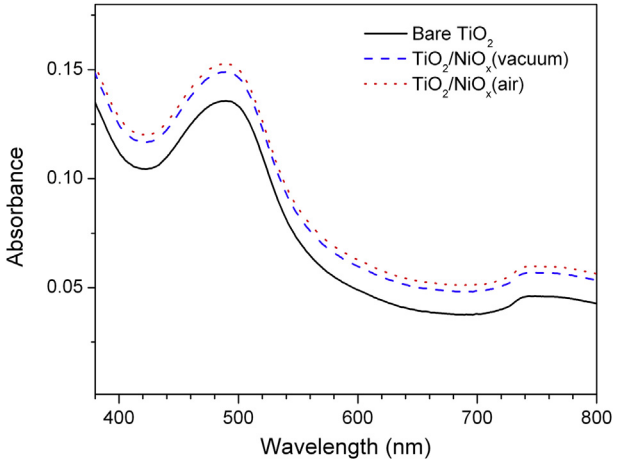

Fig. 6. Absorptions of solutions containing dyes detached from working electrodes.

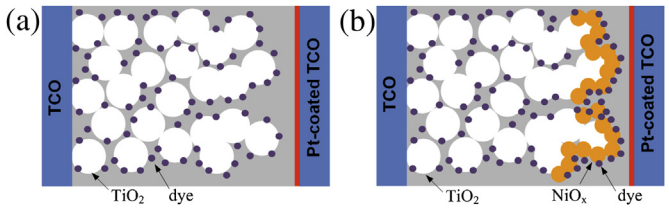

Fig. 7. Schematic drawing of working electrodes used in the present study: (a) bare TiO_2, (b) TiO_2/NiO_x.

NiO (pH 10.3) is higher than that of anatase TiO_2 (pH 6.2), indicating that the surface of the NiO_x overlayer is more basic than the TiO_2 surface [47]. The basic NiO_x-coated surface favours dye attachment through its carboxylic acid groups. Accordingly, an increase in dye adsorption upon TiO_2/NiO_x could be expected. It is noteworthy that the IEP of metallic Ni occurs at pH 3.5–4.0. Above the IEP, there is a zeta potential plateau until pH ~9, which is associated with the predominance of NiO(OH) species [48]. To distinguish between these two TiO_2/NiO_x electrodes, it is proposed that the IEP of NiO_x(air) is higher than that of NiO_x(vacuum) because the oxidative (ambient) atmosphere during heat treatment favours the formation of stoichiometric NiO. In contrast, during the sputtering process, the argon plasma enhances substantially the oxygen vacancies. The deviation from the stoichiometric NiO phase accompanies a decrease in IEP of the resultant film. The more basic TiO_2/NiO_x(air) surface leads to an increment in dye adsorption, thus resulting in better light harvesting, as compared with the TiO_2/NiO_x(vacuum) surface. To elucidate the effect of heat treatment, the chemical state of each constituent element was investigated by the X-ray photoelectron spectrum (XPS). Fig. 8(a) shows that both TiO_2/NiO_x electrodes have a major Ni($2P_{3/2}$, 853.8 eV) and a minor Ni($2P_{1/2}$, 871.6 eV) peak, respectively which are close to the value of stoichiometric NiO. A closer look at the asymmetric O_{1s} peaks in Fig. 8(b), a major peak, designated as O_I (528.8 eV), originated from lattice oxygen was dominated. However, for TiO_2/NiO_x(vacuum) electrode, a shoulder peak, designated as O_{II} (531.2 eV) after deconvolution by the Gaussian/Lorenzian method was found which may be attributed to oxygen impurities other than lattice oxygen, including physical adsorbed/chemisorbed oxygen, hydroxides within the surface layers, etc [49]. The chemisorbed oxygen onto the grain boundary form electron traps which reduce the carrier concentration considerably. By heat treatment under atmosphere, the content of O_{II} in TiO_2/NiO_x (air) electrode was declined substantially.

Electrochemical impedance spectroscopy (EIS) is a powerful technique which has been widely employed to study the kinetics of electrochemical and photoelectrochemical processes including the elucidation of salient electronic and ionic processes occurring in the DSSC [50,51]. By employing a suitable equivalent electrical circuit, one can interpret the EIS results in elucidating the effect of multilayered photoelectrodes. In this study, all EIS spectra (in Fig. 9) were recorded at open circuit voltage under illumination. Under these conditions, there is no net current flowing through the cell. All the injected electrons are recaptured by I_3^- before being extracted to the external circuit. The band bending of TiO_2 is reduced correspondingly since the electrons in the solid phases can equilibrate under illumination at open circuit [52]. Moreover, the counter electrode is always kept at equilibrium, because there is no net current flowing through it [51]. A typical equivalent circuit (EQC) was depicted in the inset of Fig. 9 which are assigned, according to the frequency range from high to low, as the ohmic serial resistance (R_s) corresponding to the electrolyte and the FTO resistance, while the resistances R_1, R_2 and R_3 are related to the charge-transfer processes occurring at the Pt counter electrode in the high-frequency region, resistance for the TiO_2/electrolyte electrode, interface, and Nernstian diffusion within the electrolyte in the low-frequency region, respectively [53]. The parameters obtained by fitting the impedance spectra with EQC are summarized in Table 4. It is obvious that R_s of the cell increased after the TiO_2 film was coated with a NiO_x overlayer, which could be attributed partly to the adverse impact by the sputtering process followed by a heat treatment on the conductivity of the FTO substrate. Furthermore, the increased impedance (R_2) as compared with the bare TiO_2 electrode showed that a NiO_x overlayer suppressed the transport of photoelectrons from TiO_2 to the electrolyte. Between the two cells, the blocking effect for TiO_2/NiO_x(vacuum) was more prominent. Li et al. [33] reported that surface modification of TiO_2 electrodes with sputtered NiO up to 21 nm in thickness reduced trap sites on TiO_2 and improved the electrochemical performance of DSSCs. However, in our study, although the back transfer of photoelectrons was suppressed for the TiO_2/NiO_x(vacuum) electrode, they might also

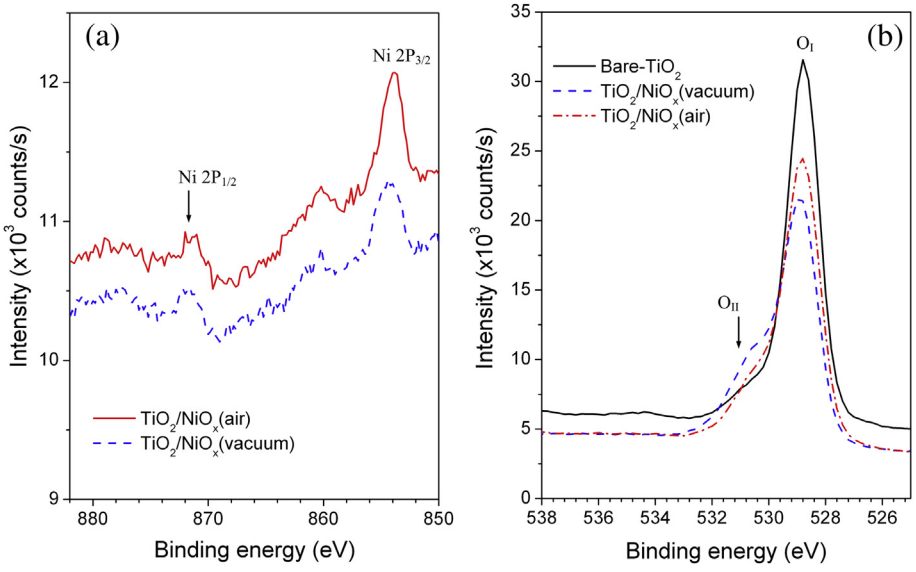

Fig. 8. XPS spectra of bare TiO_2 and TiO_2/NiO_x electrodes: (a) Ni(2p) spectra and (b) O(1s) spectra.

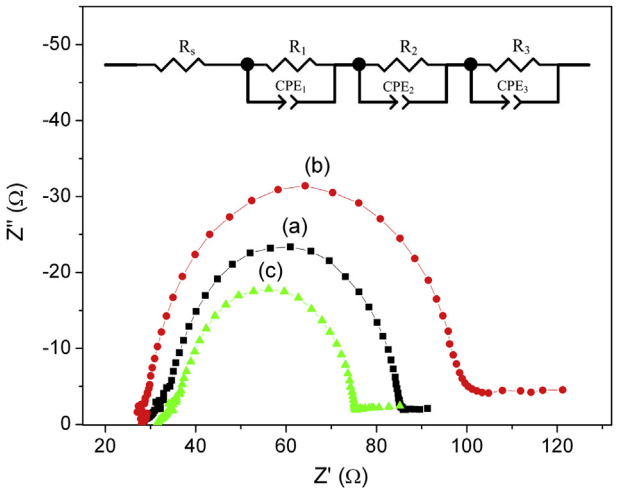

Fig. 9. Electrical impedance spectra of DSSCs fabricated from each electrode: (a) bare TiO_2, (b) TiO_2/NiO_x(vacuum) and (c) TiO_2/NiO_x(air).

Table 4
Impedance parameters determined by fitting the EIS experimental data of various electrodes to the equivalent circuit shown in Fig. 8.

	R_S (Ω)	R_1 (Ω)	R_2 (Ω)	CPE_2 (ΩF)	R_3 (Ω)
Bare TiO_2	27.68	2.07	22.09	459.1	37.22
TiO_2/NiO_x(vacuum)	29.71	8.03	58.82	518.9	48.28
TiO_2/NiO_x(air)	31.71	1.20	23.16	628.1	26.71

hinder the regeneration of oxidized dyes with iodide from electrolyte. Under this circumstance, the resultant conversion efficiency declined undesirably. In contrast, TiO_2/NiO_x(air) results in a moderate incline in R_2 as compared with that of the bare TiO_2 electrode. Finally, an enhanced photovoltaic conversion was obtained for the TiO_2/NiO_x(air) electrode. The more basic surface improves substantially both dye adsorption and moderate blocking effect in suppressing the recombination photoelectrons with electrolytes. The impedance of the CPE is given by: $Z_{CPE} = B^{-1}(i\omega)^m$, where ω is the angular frequency, B is the CPE parameter, and m ($0 \leq m \leq 1$) is the CPE exponent [54]. Generally, a CPE is used in an EQC model in place of a capacitor ($m = 1$) to compensate for the non-homogeneity in the system. For example, a rough or porous surface induces a double-layer capacitance whose behaviour could be simulated by a CPE with CPE exponent (m) value between 0.9 and 1. In our experiments, the CPE exponent of TiO_2/NiO_x(vacuum) ($m = 0.941$) is larger than the other two electrodes ($m = 0.934$ and 0.933 for TiO_2/NiO_x(air) and bare TiO_2, respectively) which could be attributed to that part of the pores and voids of TiO_2 films has been covered by sputtering. However, the thermal annealing in air restores its original porosity. The response at medium frequencies was attributed to the TiO_2|electrolyte (R_2, CPE_2 elements), since an accumulation of electrons and redox species is expected at this interface under open circuit conditions [55]. The p-type NiO_x overlayer induces more surface states and induces a positive conduction band edge movement [56]. It is rational as the photovoltage of TiO_2/NiO_x(vacuum) electrode (curve (b) in Fig. 5) declined considerably. However, owing to the effective blocking effect of TiO_2/NiO_x(air) electrode, the adverse effect of conduction band edge movement has been overcome.

4. Conclusions

In this study, a nanoporous TiO_2 electrode was fabricated by a commercial P25 paste. In order to achieve desirable conversion efficiency, a multi-layered film of 14.4 μm thick (9 layers deposited by spin-coating) was fabricated. The resultant DSSC has an optimal efficiency (η) of 6.89% with J_{sc} and V_{oc} of 22.5 mA cm^{-2} and 0.78 V, respectively. To further improve the performance, a NiO_x overlayer was deposited by reactive DC magnetron sputtering followed by heat treatment under vacuum and ambient atmosphere. SEM micrographs revealed that both voids and cavities on the bare TiO_2 and TiO_2/NiO_x(vacuum) surface could be readily diminished by annealing under ambient atmosphere. X-ray diffractograms revealed that anatase phase TiO_2 dominated in all samples and that no diffraction peaks of NiO phase could be detected for TiO_2/NiO_x(vacuum) while minor NiO reflections are present for TiO_2/NiO_x(air), even though the grazing incidence mode was carried out. The cell conversion efficiency (η) was enhanced substantially for TiO_2/NiO_x(air) by which the best η of 7.31% with J_{sc} and V_{oc} of 24.2 mA cm^{-2} and 0.80 V, respectively were obtained. Cell characteristics clearly exhibited that for TiO_2/NiO_x(air) electrode, J_{sc} was effectively improved. In contrast, a NiO_x overlayer also imparts adverse effect on cell characteristics, i.e., the fill factor (FF) declined substantially. The amount of dye adsorbed on the TiO_2 surface was determined to be 5.608×10^{-8} mol cm^{-2} for TiO_2/NiO_x(air), corresponding to an increase in dye adsorption by 10% as compared with the bare TiO_2 electrode It could be reasoned that the basic NiO_x-coated surface favours dye attachment through its carboxylic acid groups since the IEP of NiO (pH 10.3) is higher than that of anatase TiO_2 (pH 6.2). EIS analysis confirmed that a NiO_x(vacuum) overlayer suppressed effectively the transport of photoelectrons from TiO_2 to the electrolyte, while a NiO_x(air) overlayer results in only a slight decline in R_2 as compared with that of the bare TiO_2 electrode. It is proposed that the IEP of NiO_x(air) is higher than that of NiO_x(vacuum). The more basic TiO_2/NiO_x(air) surface leads to an increment in dye adsorption and as a result, facilitates the electron transport at the TiO_2/dye interface which leads to better light harvesting, as compared with the TiO_2/NiO_x(vacuum) surface.

Acknowledgements

This work was supported by the National Science Council of Taiwan, under contract no. NSC 96-2221-E-212-017.

References

[1] M. Grätzel, Nature 353 (1991) 737–739.
[2] M. Grätzel, J. Photochem. Photobiol. A 164 (2004) 3–14.
[3] M.K. Nazeeruddin, A. Kay, I. Rodicio, R. Humpbry-Baker, E. Müller, P. Liska, N. Vlachopoulos, M. Grätzel, J. Am. Chem. Soc. 115 (1993) 6382–6390.
[4] J.K. Lee, M. Yang, Mater. Sci. Eng. B 176 (2011) 1142–1160.
[5] B.A. Gregg, F. Pichot, S. Ferrere, C.L. Fields, J. Phys. Chem. B 105 (2001) 1422–1429.
[6] J. Guo, C. She, T. Lian, J. Phys. Chem. C 111 (2007) 8979–8987.
[7] J. Xia, S. Yanagida, Sol. Energy 85 (2011) 3143–3159.
[8] A. Zaban, S.G. Chen, S. Chappel, B.A. Gregg, Chem. Commun. (2000) 2231–2232.
[9] S.G. Chen, S. Chappel, Y. Diamant, A. Zaban, Chem. Mater. 13 (2001) 4629–4634.
[10] E. Palomares, J.N. Clifford, S.A. Haque, T. Lutz, J.R. Durrant, J. Am. Chem. Soc. 125 (2003) 475–482.
[11] S. Lee, J.Y. Kim, K.S. Hong, H.S. Jung, J.K. Lee, H. Shin, Sol. Energy Mater. Sol. Cells 90 (2006) 2405–2412.
[12] F. Luo, L. Wang, B. Ma, Y. Qiu, J. Photochem. Photobiol. A 197 (2008) 375–381.
[13] S. Wu, H. Han, Q. Tai, J. Zhang, S. Xu, C. Zhou, Y. Yang, H. Hu, B.L. Chen, X.Z. Zhao, J. Power Sources 182 (2008) 119–123.
[14] X. Wu, L. Wang, F. Luo, B. Ma, C. Zhan, Y. Qiu, J. Phys. Chem. C 111 (2007) 8075–8079.
[15] Z.S. Wang, M. Yanagida, K. Sayama, H. Sugihara, Chem. Mater. 18 (2006) 2912–2916.
[16] H.S. Jung, J.K. Lee, M. Nastasi, Langmuir 21 (2005) 10332–10335.
[17] S. Yang, Y. Huang, C. Huang, X. Zhao, Chem. Mater. 14 (2002) 1500–1504.
[18] Z.S. Wang, C.H. Huang, Y.Y. Huang, Y.J. Hou, P.H. Xie, B.W. Zhang, H.M. Cheng, Chem. Mater. 13 (2001) 678–682.
[19] J.H. Yum, S. Nakade, D.Y. Kim, S. Yanagida, J. Phys. Chem. B 110 (2006) 3215–3219.
[20] K.S. Ahn, M.S. Kang, J.K. Lee, B.C. Shin, J.W. Lee, Appl. Phys. Lett. 89 (2006) 013103–013105.

[21] C.B. Alcock, B. Li, J.W. Fergus, L. Wang, Solid State Ionics 53–56 (1992) 39–43.
[22] S. Berchmans, H. Gomathi, G.P. Rao, J. Electroanal. Chem. 394 (1995) 267–270.
[23] J.L. Garcia-Miquel, Q. Zhang, S.J. Allen, A. Rougier, A. Blyr, H.O. Davies, A.C. Jones, T.J. Leedham, P.A. Williamds, S.A. Impaey, Thin Solid Films 424 (2003) 165–170.
[24] S. Nandy, S. Goswami, K.K. Chattopadhyay, Appl. Surf. Sci. 256 (2010) 3142–3147.
[25] M. Yang, H. Pu, Q. Zhou, Q. Zhang, Thin Solid Films 520 (2012) 5884–5888.
[26] Y. Zhou, D. Gu, Y. Geng, F. Gan, Mater. Sci. Eng. B 135 (2006) 125–128.
[27] J. He, H. Lindström, A. Hagfeldt, S.E. Lindquist, J. Phys. Chem. B 103 (1999) 8940–8943.
[28] J. Bandara, C.M. Divarathne, S.D. Nanayakkara, Sol. Energy Mater. Sol. Cells 81 (2004) 429–437.
[29] J. Bandara, H. Weerasinghe, Sol. Energy Mater. Sol. Cells 85 (2005) 385–390.
[30] Y.M. Lee, C.H. Lai, Solid-State Electron. 53 (2009) 1116–1125.
[31] K.H. Wong, K. Ananthanarayanan, S.R. Gajjela, P. Balaya, Mater. Chem. Phys. 125 (2011) 553–557.
[32] S. Mori, S. Fukuda, S. Sumikura, Y. Takeda, Y. Tamaki, E. Suzuki, T. Abe, J. Phys. Chem. C 112 (2008) 16134–16139.
[33] L. Li, R. Chen, G. Jing, G. Zhang, F. Wu, S. Chen, Appl. Surf. Sci. 256 (2010) 4533–4537.
[34] Y. Kim, B.J. Yoo, R. Vittal, Y. Lee, N.G. Park, K.J. Kim, J. Power Sources 175 (2008) 914–919.
[35] H. Wang, Y. Liu, H. Huang, M. Zhong, H. Shen, Y. Wang, H. Yang, Appl. Surf. Sci. 255 (2009) 9020–9025.
[36] S. Ngamsinlapasathian, T. Sreethawong, Y. Suzukia, S. Yoshikawa, Sol. Energy Mater. Sol. Cells 90 (2006) 2129–2140.
[37] T. Kawashima, T. Ezure, K. Okada, H. Matsui, K. Goto, N. Tanabe, J. Photochem. Photobiol. A 164 (2004) 199–202.
[38] T. Hoshikawa, M. Yamada, R. Kikuchi, K. Eguchi, J. Electrochem. Sci. 152 (2005) E68–E73.
[39] H. Chang, H.T. Su, W.A. Chen, K.D. Huang, S.H. Chien, S.L. Chen, C.C. Chen, Sol. Energy 84 (2010) 130–136.
[40] L. Han, N. Koide, Y. Chiba, A. Islam, T. Mitate, C.R. Chim. 9 (2006) 645–651.
[41] M.A. Green, Solar Cells: Operating Principles, Technology and System Applications, first ed., Prentice-Hall, Englewood Cliffs, N.J., 1992.
[42] I. Shin, H. Seo, M.K. Son, J.K. Kim, K. Prabakar, H.J. Kim, Curr. Appl. Phys. 10 (2010) S422–S424.
[43] M.G. Kang, K.S. Ryu, S.H. Chang, N.G. Park, J.S. Hong, K.J. Kim, Bull. Korean Chem. Soc. 25 (2004) 742–744.
[44] M.C. Kao, H.Z. Chen, S.L. Young, C.Y. Kung, C.C. Lin, Thin Solid Films 517 (2009) 5096–5099.
[45] A. Kumar, P.G. Santangelo, N.S. Lewis, J. Phys. Chem. 96 (1992) 834–842.
[46] K. Kalyanasundaram, M. Grätzel, Coord. Chem. Rev. 177 (1998) 347–414.
[47] G.A. Parks, Chem. Rev. 65 (1965) 177–198.
[48] N. Hernández, R. Moreno, A.J. Sánchez-Herencia, J.L.G. Fierro, J. Phys. Chem. B 109 (2005) 4470–4474.
[49] P.C. Yao, S.T. Hang, M.J. Wu, W.T. Hsiao, Thin Solid Films 520 (2012) 2846–2854.
[50] M.C. Bernard, H. Cachet, P. Falaras, A. Hugot-Le Goff, M. Kalbac, I. Lukes, N.T. Oanh, T. Stergiopoulos, I. Arabatzis, J. Electrochem. Soc. 150 (2003) E155–E164.
[51] Q. Wang, J.E. Moser, M. Grätzel, J. Phys. Chem. B 109 (2005) 14945–14953.
[52] P.J. Cameron, L.M. Peter, J. Phys. Chem. B 107 (2003) 14394–14400.
[53] K.M. Lee, V. Suryanarayanan, K.C. Ho, Sol. Energy Mater. Sol. Cells 90 (2006) 2398–2404.
[54] A. Hauch, A. Georg, Electrochim. Acta 46 (2001) 3457–3466.
[55] C. Longo, M. De Paoli, J. Braz. Chem. Soc. 46 (2001) 889–901.
[56] J. Shi, B. Peng, J. Pei, S. Peng, J. Power Sources 193 (2009) 878–884.